

1 CNEr: a toolkit for exploring extreme 2 noncoding conservation

3

4 Ge Tan^{1,2}, Dimitris Polychronopoulos^{1,2} and Boris Lenhard^{1,2,3*}

5 ¹Computational Regulatory Genomics Group, MRC London Institute of Medical Sciences, Du
6 Cane Road, London W12 0NN, UK

7 ²Institute of Clinical Sciences, Faculty of Medicine, Imperial College London, Hammersmith
8 Campus, Du Cane Road, London W12 0NN, UK

9 ³Sars International Centre for Marine Molecular Biology, University of Bergen, Thormøhlensgate
10 55, N-5008 Bergen, Norway

11 *Corresponding author

12

13 Ge Tan: ge.tan@fgcz.ethz.ch

14 Dimitris Polychronopoulos: dimitris.polychronopoulos@genomicsengland.co.uk

15 Boris Lenhard: b.lenhard@imperial.ac.uk

16

17 Present addresses:

18 Ge Tan, Functional Genomics Center Zurich, ETH Zurich and University of Zurich,
19 Winterthurerstrasse 190, Zurich 8057, Switzerland.

20 Dimitris Polychronopoulos, Genomics England, Charterhouse Square, London EC1M 6BQ, UK.

21

22 Abstract

23 Conserved Noncoding Elements (CNEs) are elements exhibiting extreme noncoding
24 conservation in Metazoan genomes. They cluster around developmental genes and act as long-
25 range enhancers, yet nothing that we know about their function explains the observed
26 conservation levels. Clusters of CNEs coincide with topologically associating domains (TADs),
27 indicating ancient origins and stability of TAD locations. This has suggested further hypotheses
28 about the still elusive origin of CNEs, and has provided a comparative genomics-based method
29 of estimating the position of TADs around developmentally regulated genes in genomes where
30 chromatin conformation capture data is missing. To enable researchers in gene regulation and
31 chromatin biology to start deciphering this phenomenon, we developed *CNEr*, a R/Bioconductor
32 toolkit for large-scale identification of CNEs and for studying their genomic properties. We apply
33 *CNEr* to two novel genome comparisons - fruit fly vs tsetse fly, and two sea urchin genomes -
34 and report novel insights gained from their analysis. We also show how to reveal interesting
35 characteristics of CNEs by coupling *CNEr* with existing Bioconductor packages. *CNEr* is
36 available at Bioconductor (<https://bioconductor.org/packages/CNEr/>) and maintained at github
37 (<https://github.com/ge11232002/CNEr>).

38

39

40

41

42

43

44 Introduction

45 Conserved Noncoding Elements (CNEs) are a pervasive class of extremely conserved elements
46 that cluster around genes with roles in development and differentiation in Metazoa [1,2]. While
47 many have been shown to act as long-range developmental enhancers [3,4], the source of their
48 extreme conservation remains unexplained [5,6]. The need to maintain arrays of CNEs in cis to
49 the genes they regulate has led to their spatial arrangement into clusters termed Genomic
50 Regulatory Blocks (GRBs) [7,8]. The role of those clusters in genome organisation is suggested
51 by recent findings demonstrating that ancient metazoan clusters of extreme noncoding
52 conservation coincide with topologically associating domains (TADs) [9].

53
54 Numerous recent studies highlight and seek to elucidate the importance of functional non-
55 coding regions, most recently by employing the CRISPR-Cas9 based techniques to locate and
56 dissect elements that affect gene expression and phenotype/disease - associated processes
57 [10–12]. Prioritizing target loci of interest for interrogating the function of their regulatory context
58 will be one of the major focuses of functional genomic studies, as has been shown in the case
59 of the *POU5F1* locus [13], and of *NF1*, *NF2* and *CUL3* genes [14]. CNEs and the regulatory
60 landscapes defined by their clusters serve as excellent candidates for such studies [3,15,16].

61
62 A handful of CNE resources exist, mainly databases, which contain already pre-computed
63 clusters of CNEs. These databases are static and mostly not updated. A summary of these
64 resources is available in the review by Polychronopoulos et al. [6]. To our knowledge, there are
65 only two tools available for the identification of conserved elements: PFAST [17] and
66 CNEFinder [18]. The former relies on multiple sequence alignments and requires extensive
67 computation time to derive "conserved" and "non-conserved" states from a two-state
68 phylogenetic hidden Markov model (phylo-HMM), a space-time probabilistic model that

69 considers both the nucleotide substitution of each base in the genome sequence through
70 evolution and the transition from one base to the next. The latter produces CNEs based on a k-
71 mer technique for computing maximal exact matches thus finding CNEs without the requirement
72 of whole-genome alignments or indices. Neither of them comes with a comprehensive, easy-to-
73 follow suite of tools tailored to the integrated exploration of CNEs from end-to-end: from
74 identification to quality control and visualisation. Our package couples those processes
75 together, enabling the user to harness the support and wealth of packages available through the
76 common the Bioconductor infrastructure. Our package is specifically designed for efficient
77 identification of CNEs using user-specified thresholds, and it functions equally well across
78 vertebrates, invertebrates or plants. To study the evolutionary dynamics of these elements and
79 their relationship to the genes around which they cluster, it is essential to be able to both
80 produce and explore genome-wide sets of CNEs for a large number of species comparisons in
81 a dedicated workflow, each with multiple length and conservation thresholds.

82

83 The *CNEr* package aims to detect CNEs and visualise them along the genome under a unified
84 framework. For performance reasons, the implementation of CNE detection and corresponding
85 I/O functions are primarily written as C extensions to R. We have used *CNEr* to produce sets of
86 CNEs by scanning pairwise whole-genome net alignments with multiple reference species, each
87 with two different window sizes and a range of minimum identity thresholds, available at
88 <http://ancora.genereg.net/downloads>. In this work, we demonstrate the application of *CNEr* to
89 the investigation of noncoding conservation between fruit fly *Drosophila* and tsetse fly *Glossina* -
90 the two species at the evolutionary separation not previously investigated in insects [7] - and
91 between two species of sea urchins. This has enabled us to observe some properties of GRB
92 target genes shared across Metazoa. In a previous study, we showed that more distant
93 comparisons in Diptera (between *Drosophila* and mosquitoes) failed to identify CNEs [7]. On the
94 other hand, the conservation level across different species of the *Drosophila* genus is

95 comparable to that across placental mammals. With *Drosophila* and *Glossina*, we wanted to
96 explore the evolutionary divergence comparable to human vs. fish in another lineage and
97 establish whether it is the same functional class of genes that is accompanied by CNEs
98 featuring such a deep level of conservation. In the case of sea urchins, we wanted to investigate
99 a lineage at an intermediate distance to vertebrates - closer than insects, more distant than the
100 early branching chordates - in order to establish the continuum of GRBs across Metazoa. We
101 present a series of downstream analysis of the newly identified CNEs, identifying their
102 characteristic sequence features in invertebrates and functional classes of genes whose loci
103 they span.

104 Design and Implementation

105 Overview of *CNEr* workflow

106 *CNEr* provides the functionality of large-scale identification and advanced visualisation of CNEs
107 based on our previous strategies of detecting CNEs [7,8,19] as shown in Fig 1. *CNEr* scans the
108 whole genome pairwise net alignment, which can be downloaded from UCSC or generated by
109 the *CNEr* pipeline, for conserved elements. Various quality controls of the alignments are
110 provided. The composition of aligned bases in the alignment can be used for tuning parameters
111 during pairwise alignment (S1 Fig). More closely related species are expected to give higher
112 rates of matched bases. The syntenic dotplot of the alignments (S2 Fig) quickly shows the
113 syntenic regions between two assemblies.

114

115 **Fig 1: *CNEr* workflow.**

116 (A) A typical pipeline of identification and visualisation of CNEs. (B) Illustration of scanning an
117 alignment for CNEs. The scanning window moves along the alignment for conserved regions.
118 The exons and repeats regions are skipped during the scanning by default.

119
120 Considering the different extents of evolutionary divergence and sequence similarity between
121 assemblies, we typically use the identity thresholds of 70% to 100% identity over a scanning
122 window of 30 bp or 50 bp. Known annotations of exons and repeats are compiled from sources
123 such as UCSC [20] and Ensembl [21] for common genomes, and elements overlapping with
124 these regions are typically skipped during the scanning. Genome annotation pipeline, such as
125 MAKER [22], can be used to create annotations for new genome assemblies.

126
127 Net alignments only keep the best match for each region in the reference genome. This is not
128 acceptable when one of the aligned genomes underwent one or more whole genome
129 duplications, leading to legitimate deviations from 1:1 orthology for many CNEs. To eliminate
130 the bias of the choice of reference genome in the alignment and to capture duplicated CNEs
131 during whole genome duplication (WGD), we scan two sets of net alignments by using each of
132 the two compared genomes as reference in turn. This strategy performs well when comparing
133 species with different numbers of WGD rounds, such as tetrapod vertebrates against teleost fish
134 [23], or common carp [24] against other teleost fish. In such cases, some of the identified CNE
135 pairs from two rounds of screening do overlap on both assemblies, and hence are merged into
136 one CNE pair. As the last step, we align the CNEs back to the two respective genomes using
137 BLAT and discard the ones with high number of hits. The remaining elements are considered to
138 be a reliable set of CNEs.

139
140 *CNEr* provides a quick overview of the genomic distribution of CNEs along chromosomes. In S3
141 Fig, each CNE between human and mouse is plotted relative to each human chromosome (x-

142 axis). We plot the cumulative number of CNEs over chromosomal positions. A CNE cluster is
143 represented as a sharp increase of height in y-axis with small change in x-axis. For visualisation
144 of CNEs in any genome browser, *CNEr* can export the CNE coordinates in BED file format and
145 CNE density (measured by the percentage of area covered by CNEs within a smoothing
146 window) in **bedGraph** and **bigWig** formats. Since running the whole pipeline of CNE detection
147 can be time-consuming, we also implemented a storage and query system with SQLite as
148 backend. Based on the visualisation capability of the *Gviz* package [25], *CNEr* can produce
149 publication-quality horizon plots of CNE density along with other genomic annotations (see
150 Methods and Data). Examples of the horizon plots are given in the following sections.

151 *CNEr* package implementation

152 *CNEr* is a Bioconductor package developed in R statistical environment, distributed under the
153 GPL-2 licence for *CNEr* code, and UCSC Kent's licence for Jim Kent's C source code it builds
154 on [20]. Although *CNEr* supports compilation for both 32-bit and 64-bit systems across multiple
155 platforms, it has limited functionality on the Windows platform due to the lack of the external
156 sequence alignment software *BLAT* [26], which is required in the pipeline.

157 Overview of whole genome pairwise alignment pipeline

158 UCSC Genome Informatics (<http://hgdownload.soe.ucsc.edu/downloads.html>) provides the
159 pairwise alignments between many popular species. However, there is a frequent need to
160 produce pairwise alignments for novel genome assemblies for new species, or using specific
161 assembly versions when they are not available from UCSC. This pipeline mostly requires
162 external sequence aligners and UCSC Kent's utilities [20], and provides well-tested parameters
163 for species with a varying degree of evolutionary divergence. In brief, first a sequence alignment
164 software, *LASTZ* [27] or *LAST* [28], is used to find the similar regions between two repeat-

165 masked genomes. Then, if two neighbouring alignments are close enough in the genome, they
166 are joined into one fragment. During the alignment, every genomic fragment can match several
167 others, and the longest one is kept. Finally, blocks of alignments are grouped into stretches of
168 synteny and form the so called "net" alignments in Axt format [29]. *CNEr* comes with a vignette
169 to demonstrate the whole pipeline. The produced Axt alignment can be manipulated in R as the
170 *Axt* class, which is extended from *GRangePairs* class defined in *CNEr* (see S2 Text).

171 Overview of the Axt scanning algorithm

172 The Axt alignment scanning algorithm constitutes the central part of this package for the
173 identification of conserved noncoding elements. Due to the massive manipulation of characters,
174 we implemented this algorithm purely in C for performance reasons; it is available to the R
175 environment through R's C interface. The minimal input is the Axt alignment and the ranges to
176 filter out, i.e., the coding and/or repeat masked regions.

177

178 The Axt screening algorithm proceeds as in S1 Algorithm. First, the Axt alignment is converted
179 into a linked Axt data structure as implemented in Jim Kent's UCSC source code [20]. The
180 filtering ranges are encoded into a hash table, where keys are the chromosome/sequences
181 names and values are pointers to the linked lists of coordinates ranges. We then iterate over the
182 linked Axt alignments. For each alignment, we use a running window to scan the alignment with
183 a step size of 1 bp. Each base is searched against the filtering hash table and matched bases
184 are skipped. All segments above the identity threshold are kept. The overlapping segments are
185 merged into larger pieces. This procedure produces a set of CNEs conserved between the two
186 aligned genome assemblies.

187 *CNEr* visualisation capability

188 Instead of using the standard density plot for CNE density (as implemented in e.g. the Ancora
189 browser), we introduce the horizon plot with the aim to increase the dynamic range of CNE
190 density visualisation. The horizon plot provides a way of visualising CNE density over several
191 orders of magnitude, and eliminates the need for multiple standard density tracks at different
192 thresholds along the genomic coordinates. Instead, a relatively low conservation threshold is
193 used, and multiple overlaid sections of the horizon plots will reveal peaks with different
194 conservation density (see Fig 3A and Fig 3B in horizon plot, Fig 3C and Fig 3D in Ancora
195 browser). We expand the functionality of "horizonplot" in *latticeExtra* package and integrate it
196 into *Gviz* [25], which is the plot engine used in *CNEr*.

197 Results

198 *CNEr* use case I: *Drosophila-Glossina* CNEs

199 Here we demonstrate the application of *CNEr* to the analysis of Tsetse Fly (*Glossina morsitans*)
200 CNEs and their putative target genes. *Glossina* is the sole vector of African trypanosomiasis
201 ("sleeping sickness"), and it mediates transmission of the disease during feeding on blood. It
202 has been shown previously [7] that, while there are tens of thousands of CNEs detected across
203 different *Drosophila* species, there are almost no highly conserved elements found between
204 *Drosophila* and malaria mosquito *Anopheles gambiae* or other mosquitos. *Glossina* and
205 *Drosophila* are much closer to each other than either of them is to mosquitos, having a common
206 ancestor that has diverged around 60.3 Mya (S4 Fig). With the recently available assembly and
207 gene annotation of *Glossina* [30] (see S1 Text), we were able to identify clusters of CNEs
208 between these two species. The clusters correspond to a subset of clusters defined by the

209 CNEs derived from comparisons of different *Drosophila* species. A further investigation of gene
210 functions, which are retained or missing in *Glossina*, was carried out by comparison with the
211 *Drosophila* clusters.

212

213 A summary of CNEs detected between *Glossina* and *Drosophila* is given in Table 1. As
214 expected, many fewer CNEs are detected from the comparison between *Glossina* and
215 *Drosophila* than between any two *Drosophila* species, since *Glossina* is an outgroup to the
216 *Drosophila/Sophophora* family. A closer examination of the CNE density plot in Ancora browser
217 [31] revealed many missing clusters of CNEs relative to CNE density across *Drosophila*
218 species, especially at a more stringent threshold. We wanted to find out if the missing and
219 retained CNE clusters differ with respect to the functional categories of the genes they span. In
220 the following analysis, the CNEs that are conserved for more than 70% over 30 bp are
221 considered.

222

Table 1: The number of CNEs between *D. melanogaster* and several other species,
including *G. morsitans*

Minimum identity	vs <i>D.</i> <i>ananassae</i>	vs <i>D.</i> <i>pseudoobscura</i>	vs <i>D.</i> <i>mojavensis</i>	vs <i>D.</i> <i>virilis</i>	vs <i>G.</i> <i>morsitans</i>
70% over 30 bp	NC	NC	176366	204970	9691
80% over 30 bp	NC	313570	127293	146793	3924
90% over 30 bp	NC	212951	81436	92288	1922
96% over 30 bp	177759	128843	47408	52134	813

100% over 30 bp	112073	76715	26972	29445	414
70% over 50 bp	266385	248357	104476	120628	3185
80% over 50 bp	223975	177266	66063	75204	1796
90% over 50 bp	142899	96994	33455	37098	732
96% over 50 bp	79631	49380	16387	17831	244
98% over 50 bp	55460	33463	10741	11548	150
100% over 50 bp	29218	17201	5250	5585	66

NC, not counted due to the threshold being too low for close species.

223

224 The most deeply conserved vertebrate CNEs are usually associated with genes involved in
225 transcriptional regulation or development (trans-dev) functions [19]. Due to high divergence
226 between *Drosophila* and *Glossina*, the regions with detectable CNE arrays tend to be of low
227 CNE turnover, i.e. the process of sequence divergence and loss of ancestral CNEs is slow. If
228 the same functional subset of genes is surrounded by low-turnover CNE clusters as in
229 vertebrates, the encompassed genes will more likely be essential key developmental genes [5].
230 Indeed, *Drosophila* genes associated with (i.e. nearest to) *Glossina* vs. *Drosophila* CNEs are
231 also associated with trans-dev terms (Fig 2A). Development, including organ, system and tissue
232 development, appears at the majority of the top Gene Ontology (GO) terms. The other highly
233 significant GO terms include biological regulation, regulation of cellular process and cell
234 differentiation. CNE clusters can span regions of tens to hundreds of kilobases around the
235 actual target gene, which is on average shorter than the equivalent spans in vertebrate
236 genomes. This is in agreement with our observation that CNE clusters and the GRBs they

237 define (and, by extension, the underlying TADs) expand and shrink roughly in proportion to
238 genome size [9]. The *H15* and *mid* locus (Fig 3A) is one of the biggest CNE clusters retained
239 between *Glossina* and *Drosophila*. The *H15* and *mid* genes encode the T-box family proteins
240 involved in heart development [32]. Although the CNE density between *Drosophila* and *Glossina*
241 is much lower than that across the *Drosophila* genus, it clearly marks the CNE cluster
242 boundaries of this locus, containing 67 CNEs at the 70% identity over 30 bp threshold. For the
243 40 largest retained CNE clusters, we provide a comprehensive list of CNE cluster coordinates,
244 the target genes, the protein domains and the number of associated CNEs (S1 Table). As we
245 can see, the majority of the target genes have *Homeobox*, *Forkhead* or *C2H2* Zn finger
246 domains, just like the genes spanned by the most conserved CNE clusters in vertebrates.

247

248 **Fig 2: Over-represented GO Biological Process terms ranked by GeneRatio.**

249 The gene ratio is defined as the number of genes associated with the term in our selected
250 genes divided by the number number of selected genes. The p-values are adjusted using "BH"
251 (Benjamini-Hochberg) correction. The visualisation is done by *clusterProfiler* [33]. (A) GO
252 enrichment for genes nearest to *Drosophila* and *Glossina* CNEs. (B) GO enrichment for genes
253 in the missing CNEs clusters compared between *Drosophila* and *Glossina*.

254

255 **Fig 3: Horizon plot of CNE density around key developmental genes along *D. melanogaster* as reference.**

257 (A) *H15* and *mid* genes are spanned by arrays of CNEs. Despite the much lower CNE density
258 from *D. melanogaster* and *Glossina*, a CNE cluster boundary shows up that is consistent with
259 CNEs from other *drosophila* species. (B) The CNE cluster around *ct* gene is missing in the
260 comparison of *D. melanogaster* and *Glossina* since no CNEs are detected. This implies that this
261 region undergoes a higher CNE turnover rate. (C, D) The same loci as in (A, B) are shown on
262 the Ancora browser in order to compare the normal CNE density plot with the horizon plot.

263 Notations: ensGene, Ensembl gene track; *Glossina* 21/30, *G. morsitans* 70% identity over 30
264 bp; droAna2 49/50, *D. ananassae* 98% identity over 50 bp; dp3 48/50, *D. pseudoobscura* 96%
265 identity over 50 bp; droMoj2 48/50, *D. mojavensis* 96 % identity over 50 bp; droVir2 48/50, *D.*
266 *virilis* 96% identity over 50 bp.

267

268 Some other regions have strong clusters of CNEs conserved among *Drosophila* species,
269 however, the CNE cluster between *Drosophila* and *Glossina* is absent. The *ct* locus (Fig 3B),
270 encoding the cut transcription factor, is one of the best representative cases. Ct plays roles in
271 the later stages of development, controlling axon guidance and branching in the development of
272 the nervous system, as well as in the specification of several organ structures such as
273 Malpighian tubules [34]. In order to locate the CNE clusters missing from *Drosophila* vs.
274 *Glossina* comparison, we use the CNE clusters detected in *D. melanogaster* vs. *D. ananassae*
275 comparison as reference and compare them with the aforementioned retained CNE clusters.
276 The genes within those missing CNE clusters are highly enriched for axon guidance and
277 neuronal development (Fig 2B). We then examine the CNE turnover rate (the speed of replacing
278 old CNEs) of the 216 human genes that are associated with the axon guidance term
279 (GO:0007411), with both human and *Drosophila* as reference. The turnover rate is calculated as
280 the reduction of the number of CNEs between two sets of CNEs. For human reference, we
281 choose the CNE set of human vs. mouse and human vs. zebrafish, while *D. melanogaster* vs.
282 *D. ananassae* and *D. melanogaster* vs. *Glossina* are chosen for *Drosophila* reference. As
283 shown in Fig 4, the axon guidance genes have significantly higher turnover rate than the other
284 genes ($p < 1e-5$, Kolmogorov-Smirnov one-sided test) in both human and *Drosophila* lineages.

285

286 **Fig 4: Cumulative distribution function of the changes of CNE number.**

287 For a 40kb window around each orthologous gene pair between human and *drosophila*, we
288 calculate the reduction of the number of CNEs for human (# of CNEs from human-mouse

289 comparison minus # of CNEs from human-zebrafish comparison) and drosophila (# of CNEs
290 from *D. melanogaster* vs. *D. ananassae* comparison minus # of CNEs from *D. melanogaster* vs.
291 *Glossina*) as reference. The axon guidance genes significantly show a higher degree of CNE
292 number reduction, compared with the other genes ($p < 1e-5$, Kolmogorov-Smirnov one-sided
293 test).

294 *CNEr* use case II: sea urchin CNEs

295 In this section we apply *CNEr* to the comparison of highly fragmented genome assemblies of
296 two sea urchin species *Strongylocentrotus purpuratus* and *Lytechinus variegatus* (see S1 Text).
297 The purpose of this analysis is twofold. First, we want to demonstrate how well *CNEr* is able to
298 call CNEs and their clusters in the case of highly fragmented draft genomes: the ability to
299 perform this analysis on draft genome assemblies would show that our approach can be applied
300 to a large number of available genomes, most of which haven't been assembled past the draft
301 stage and are likely to remain in that state. Second, we wanted to ask if a third lineage,
302 evolutionarily closer to vertebrates than insects but still lacking any shared CNEs with
303 vertebrates, would exhibit the same patterns of noncoding conservation. This could provide a
304 hint towards CNEs' universal presence in Metazoa, in addition to providing an informative
305 additional dataset for comparative studies of genomic regulatory blocks.

306
307 *S. purpuratus* is a popular model organism in cell and developmental biology. *S. purpuratus* and
308 *L. variegatus* have a divergence time of 50 Mya [35] and historically moderate rates of
309 sequence divergence, which makes them ideal for comparative genomics studies of regulatory
310 elements. We identified 18,025 CNEs with threshold of 100% identity over 50 bp window.
311 Despite the highly fragmented assemblies, we could clearly detect 808 prominent CNE clusters.
312

313 An especially interesting observation is the largest cluster we detected, at the *Meis* gene locus
314 (Fig 5). The CNE density clearly marks the boundaries of the CNE cluster. In Metazoa, *Meis*,
315 one of the most well-known homeobox genes, is involved in normal development and cell
316 differentiation. Tetrapod vertebrates have three *Meis* orthologs as a result of two rounds of
317 whole genome duplication. The CNE cluster around *Meis2* (one of three *Meis* paralogs arisen
318 by two WGD rounds at the root of vertebrates) is the largest such cluster in vertebrates [19].
319 Remarkably, the cluster of CNEs around *Drosophila's Meis* ortholog, *hth* (homothorax), is also
320 the largest CNE cluster in the *D. melanogaster* genome [7]. It is currently unknown why the
321 largest clusters of deeply conserved CNEs are found around the same gene in three different
322 metazoan lineages, even though none of the CNEs from one lineage has any sequence
323 similarities to CNEs in the other two. The most plausible explanation is that the ancestral *Meis*
324 (*hth*) locus was already the largest such locus in the ancestral genome, and that CNE turnover
325 has led to three separate current lineage-specific sets of CNEs.

326

327 **Fig 5: Horizon plot of CNE density at *Meis* loci on sea urchin *Strongylocentrotus***
328 ***purpuratus*.**

329 The density plots of CNEs detected at similarity threshold 96% (48/50), 98% (49/50) and 100%
330 (50/50) over 50 bp sliding window, in *Lytechinus variegatus* comparison, are shown in three
331 horizon plot tracks. The boundaries of CNE clusters from various thresholds are mutually
332 consistent.

333

334 *CNEr* reveals interesting sequence features characteristic of
335 ultraconservation

336 It has been shown that vertebrate nonexonic CNEs are enriched in the TAATTA hexanucleotide
337 motif, which is an extended recognition site for the homeodomain DNA-binding module [36].
338 With *CNEr*, we can easily verify the existence of TAATTA motif in CNEs of invertebrate species.
339 In S5 Fig A, we consider CNEs identified by *CNEr* that are conserved between *D. melanogaster*
340 and *D. virilis* over 98% for more than 50 nucleotides and plot them by increasing width using
341 *heatmaps* package (<https://bioconductor.org/packages/heatmaps/>). The first two heatmaps
342 confirm that CNEs are enriched in AT inside but exhibit a marked depletion of AT at their
343 borders, consistent with what is known about their biology in vertebrates [37]. Furthermore, the
344 TAATTA motif is enriched in insect CNEs. The motif seems to be extended further by flanking
345 A/T nucleotides. When replacing A/T (W) with G/C (S), the heatmap pattern disappears. We ask
346 whether this is a general property of CNEs in Metazoa and, using *CNEr*, proceed to the
347 identification of CNEs that are conserved between (a) *C. elegans* and *C. briggsae* at 100% for
348 more than 30 nucleotides (worm CNEs, see S5 Fig B), (b) *L. variegatus* and *S. purpuratus* at
349 100% for more than 50 nucleotides (sea urchin CNEs, see S5 Fig C). We observe that the same
350 pattern does not hold in those cases, i.e. it appears like enrichment of CNEs in TAATTA is not a
351 universal phenomenon but applies only to insect and vertebrate elements. Our pipeline is a
352 powerful tool for studying the question of how and when this TAATTA-enrichments originated,
353 as well as a multitude of related questions.

354

355 Downstream overlap analysis of CNEs reveals that they are 356 highly enriched in stem-cell regulatory elements

357 Finally, we demonstrate the utility of *CNEr* for general hypothesis generation about CNEs by
358 identifying elements highly conserved (>98% identity over 50 bp) between human and chicken
359 and performing global and pairwise overlap analyses against various genomic features using
360 the R/Bioconductor packages *LOLA* [38] and *regioneR* [39], respectively. *LOLA* allows for
361 enrichment analysis of genomic intervals using a core reference database assembled from
362 various resources of genomic data, while *regioneR* permits cross-validation of the findings
363 through pairwise overlap analyses. As evident from inspection of S2 Table and Fig 6, both
364 packages converge to the conclusion that the identified CNEs between human and chicken are
365 significantly enriched in *Sox2* and *Oct-4 (POU5F1)* binding sites. *Sox2* and *Oct-4*, in concert
366 with *Nanog*, are believed to play key roles in maintaining pluripotency. This finding comes in
367 accordance with previous reports suggesting that several CNEs are enriched in classical
368 octamer motifs recognized by developmental homeobox transcription factors [40]. Nonetheless,
369 this is the first time that such an association of the most deeply conserved CNEs with key
370 pluripotency elements is reported in the literature, and we anticipate that more associations of
371 this kind will be revealed in the future by coupling *CNEr* with other R/Bioconductor packages.

372

373 **Fig 6: Pairwise overlap analysis of CNEs demonstrates association with *Sox2*, *POU5F1*** 374 **and *Nanog* binding regions.**

375 In all three cases, permutation tests with 1000 permutations of CNEs are shown. In grey the
376 number of overlaps of the randomized regions with the test regions of interest (in this case,
377 *Sox2*, *POU5F1* and *Nanog*) are depicted. Those overlaps of the randomized regions cluster
378 around the black bar that represents the mean. In green, the number of overlaps of the actual

379 regions (CNEs in this case) with the test regions is shown and is proved to be much larger than
380 expected in all cases. The red line denotes the significance limit.

381 Availability and Future Directions

382 The *CNEr* package with self-contained UCSC Kent's utility source code is available at
383 Bioconductor release branch <http://bioconductor.org/packages/CNEr/>. Active development and
384 bug reports is hosted on github <https://github.com/ge11232002/CNEr/>. Currently the *BLAT* is the
385 only supported aligner for identifying repeats. Other high performance short read aligners that
386 run in parallel, such as Bowtie1/2 and BWA, are desired for large set of CNEs. Furthermore,
387 integration of GRB identification approach and GRB target gene prediction is planned for future
388 development.

389 Declarations

390 Competing interests

391 The authors declare that they have no competing interests.

392 Funding

393 GT and BL were supported by EU project ZF-Health (FP7/2010-2015 grant agreement 242048)
394 and Wellcome Trust (award P55504_WCMA). Medical Research Council has provided the
395 support for DP and BL (award MC_UP_1102/1).

396 Authors' contributions

397 GT and BL conceived the project. GT implemented the software, analyzed the data. DP tested
398 the software, analyzed data. GT, DP, BL wrote the manuscript.

399 Acknowledgements

400 We are grateful to the Bioconductor community for trying out the *CNEr* package and providing
401 useful input.

402 Supporting information

403 S1 Text. Glossina and sea urchin data.

404 S2 Text. Working with Paired Genomic Ranges

405 S1 Fig. The heatmap shows the percentage of matched bases in
406 the Axt alignments.

407 This can be useful for examining the quality of Axt alignments, especially from the whole
408 genome pairwise alignment pipeline in *CNEr* package. The left panel has higher rates of
409 matches than right panel since the divergence of human and mouse is much smaller than that
410 between human and zebrafish.

411 **S2 Fig. The syntenic plot of alignment blocks between chr1, chr2**
412 **of human and chr1, chr2 of mouse.**

413 This plot is mostly used for tuning the parameters during whole genome pairwise alignment to
414 get better alignments. It can also show ancient duplications for the alignment of a sequence
415 against itself.

416 **S3 Fig. The distribution of CNEs along the 6 biggest**
417 **chromosomes in human genome.**

418 Each CNE is plotted as a dot with the position in chromosome as x-axis. A sharp increase in y-
419 axis represents a CNE cluster.

420 **S4 Fig. The species tree of Drosophila, Glossina and mosquitos.**

421 The phylogenetic tree is constructed based on the data on last common ancestors from
422 TimeTree (Hedges et al., 2006). The genome of the malaria mosquito *A. gambiae* is highly
423 divergent from *Drosophila* family and unsuitable for comparative genomics study, while *G.*
424 *morsitans* is much closer.

425 **S5 Fig . Sequence heatmaps of CNEs in different lineages.**

426 (A) *D. melanogaster* and *D. virilis* (B) *C. elegans* and *C. briggsae* (C) *L. variegatus* and *S.*
427 *purpuratus*. The CNEs are ranked by decreasing CNE width.

428 S1 Table. A list of the most prominent CNE clusters detected
429 between *Drosophila* and *Glossina*.

430 S2 Table. Overlap analysis of CNEs.

431 Global overlap analysis of CNEs against multiple genomic features using LOLA reveals that
432 they overlap with Nanog, Sox2 and POU5F1 binding regions. This table is the output of
433 runLOLA algorithm sorted by FDR. All top hits include important factors associated with
434 pluripotency. userSet: all CNEs conserved between human and chicken over 98% identity for
435 more than 50 bp. collection: all elements in CODEX database. universe: all active DNase I
436 hypersensitive sites.

437 S1 Algorithm. The algorithm of scanning Axt alignment.

438
439 **References:**

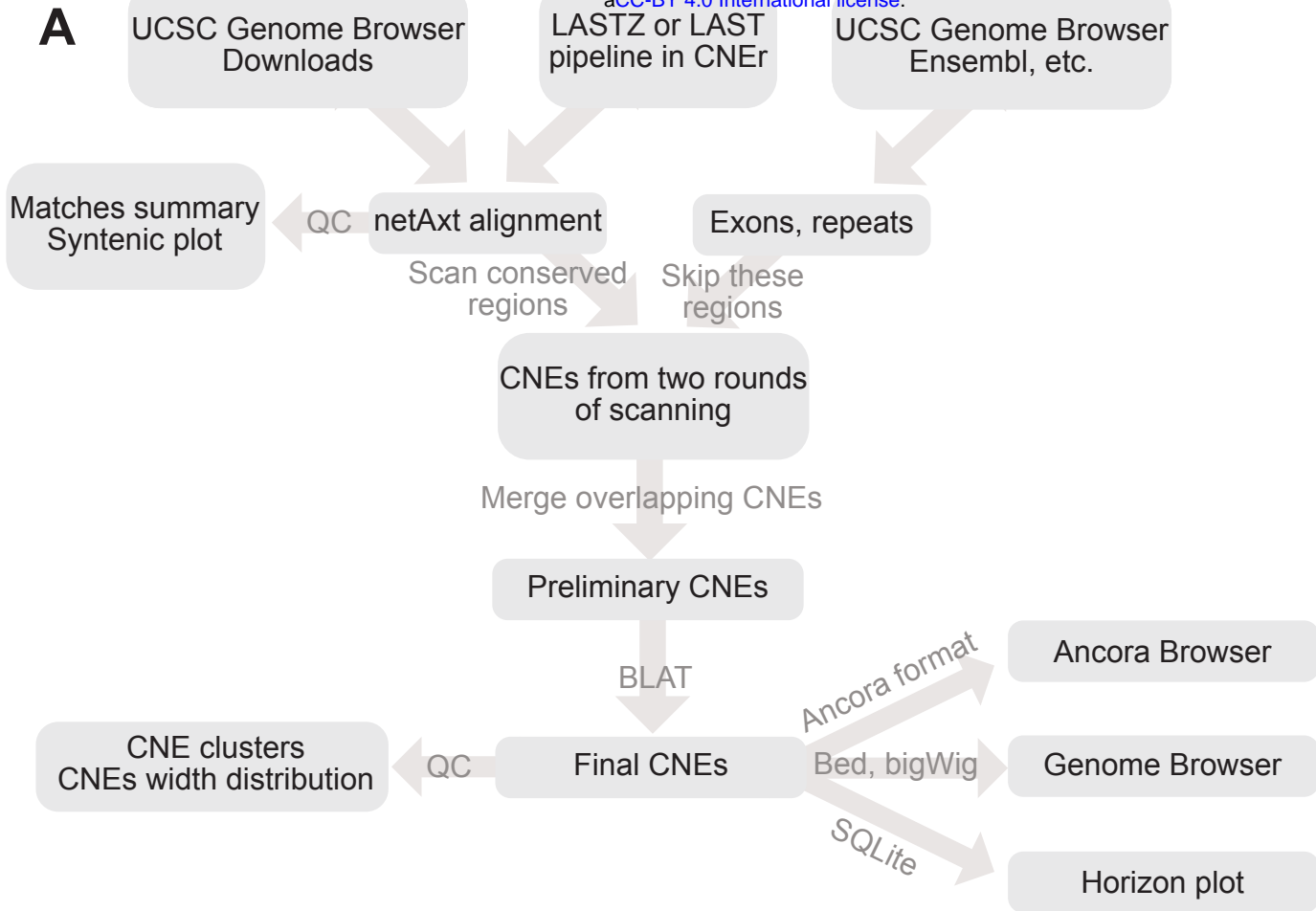
- 440 1. Woolfe A, Goodson M, Goode DK, Snell P, McEwen GK, Vavouri T, et al. Highly conserved
441 non-coding sequences are associated with vertebrate development. PLoS Biol. 2005;3: e7.
- 442 2. Bejerano G, Pheasant M, Makunin I, Stephen S, Kent WJ, Mattick JS, et al. Ultraconserved
443 elements in the human genome. Sci. 2004;304: 1321–1325.
- 444 3. de la Calle-Mustienes E, Feijóo CG, Manzanares M, Tena JJ, Rodríguez-Seguel E, Letizia
445 A, et al. A functional survey of the enhancer activity of conserved non-coding sequences
446 from vertebrate Iroquois cluster gene deserts. Genome Res. 2005;15: 1061–1072.
- 447 4. Pennacchio LA, Ahituv N, Moses AM, Prabhakar S, Nobrega MA, Shoukry M, et al. In vivo
448 enhancer analysis of human conserved non-coding sequences. Nature. 2006;444: 499–
449 502.
- 450 5. Harmston N, Baresic A, Lenhard B. The mystery of extreme non-coding conservation.
451 Philos Trans R Soc London Ser B, Biol Sci. 2013;368: 20130021.
- 452 6. Polychronopoulos D, King JWD, Nash AJ, Tan G, Lenhard B. Conserved non-coding
453 elements: developmental gene regulation meets genome organization. Nucleic acids Res.
454 2017;45: 12611–12624.
- 455 7. Engström PG, Ho Sui SJ, Drivenes O, Becker TS, Lenhard B. Genomic regulatory blocks
456 underlie extensive microsynteny conservation in insects. Genome Res. 2007;17: 1898–
457 1908.
- 458 8. Kikuta H, Laplante M, Navratilova P, Komisarczuk AZ, Engström PG, Fredman D, et al.
459 Genomic regulatory blocks encompass multiple neighboring genes and maintain conserved

- 460 synteny in vertebrates. *Genome Res.* 2007;17: 545–555.
- 461 9. Harmston N, Ing-Simmons E, Tan G, Perry M, Merckenschlager M, Lenhard B. Topologically
462 associating domains are ancient features that coincide with Metazoan clusters of extreme
463 noncoding conservation. *Nat Commun.* 2017;8: 441.
- 464 10. Mumbach MR, Satpathy AT, Boyle EA, Dai C, Gowen BG, Cho SW, et al. Enhancer
465 connectome in primary human cells identifies target genes of disease-associated DNA
466 elements. *Nat Genet.* 2017;49: 1602–1612.
- 467 11. Montalbano A, Canver MC, Sanjana NE. High-Throughput Approaches to Pinpoint Function
468 within the Noncoding Genome. *Mol cell.* 2017;68: 44–59.
- 469 12. Wright JB, Sanjana NE. CRISPR Screens to Discover Functional Noncoding Elements.
470 *Trends Genet TIG.* 2016;32: 526–529.
- 471 13. Diao Y, Li B, Meng Z, Jung I, Lee AY, Dixon J, et al. A new class of temporarily phenotypic
472 enhancers identified by CRISPR/Cas9-mediated genetic screening. *Genome Res.* 2016;26:
473 397–405.
- 474 14. Sanjana NE, Wright J, Zheng K, Shalem O, Fontanillas P, Joung J, et al. High-resolution
475 interrogation of functional elements in the noncoding genome. *Sci.* 2016;353: 1545–1549.
- 476 15. Royo JL, Bessa J, Hidalgo C, Fernández-Miñán A, Tena JJ, Roncero Y, et al. Identification
477 and analysis of conserved cis-regulatory regions of the MEIS1 gene. *PloS one.* 2012;7:
478 e33617.
- 479 16. Anderson E, Devenney PS, Hill RE, Lettice LA. Mapping the Shh long-range regulatory
480 domain. *Dev.* 2014;141: 3934–3943.
- 481 17. Hubisz MJ, Pollard KS, Siepel A. PHAST and RPHAST: phylogenetic analysis with
482 space/time models. *Briefings Bioinforma.* 2011;12: 41–51.
- 483 18. Ayad LAK, Pissis SP, Polychronopoulos D. CNEFinder: finding conserved non-coding
484 elements in genomes. *Bioinformatics (Oxford, England).* 2018. pp. i743–i747.
- 485 19. Sandelin A, Bailey P, Bruce S, Engström PG, Klos JM, Wasserman WW, et al. Arrays of
486 ultraconserved non-coding regions span the loci of key developmental genes in vertebrate
487 genomes. *BMC Genomic-.* 2004;5: 99.
- 488 20. Kent WJ, Sugnet CW, Furey TS, Roskin KM, Pringle TH, Zahler AM, et al. The human
489 genome browser at UCSC. *Genome Res.* 2002;12: 996–1006.
- 490 21. Yates A, Akanni W, Amode MR, Barrell D, Billis K, Carvalho-Silva D, et al. Ensembl 2016.
491 *Nucleic acids Res.* 2016;44: D710–D716.
- 492 22. Cantarel BL, Korf I, Robb SMC, Parra G, Ross E, Moore B, et al. MAKER: an easy-to-use
493 annotation pipeline designed for emerging model organism genomes. *Genome Res.*
494 2008;18: 188–196.
- 495 23. Jaillon O, Aury J-M, Brunet F, Petit J-L, Stange-Thomann N, Mauceli E, et al. Genome
496 duplication in the teleost fish *Tetraodon nigroviridis* reveals the early vertebrate proto-
497 karyotype. *Nature.* 2004;431: 946–957.
- 498 24. Kolder ICRM, van der Plas-Duivesteyn SJ, Tan G, Wiegertjes GF, Forlenza M, Guler AT, et
499 al. A full-body transcriptome and proteome resource for the European common carp. *BMC*
500 *Genomic-.* 2016;17: 701.
- 501 25. Hahne F, Ivanek R. Visualizing Genomic Data Using Gviz and Bioconductor. *Methods Mol*
502 *Biol.* 2016;1418: 335–351.
- 503 26. Kent WJ. BLAT--the BLAST-like alignment tool. *Genome Res.* 2002;12: 656–664.
- 504 27. Schwartz S, Kent WJ, Smit A, Zhang Z, Baertsch R, Hardison RC, et al. Human-mouse
505 alignments with BLASTZ. *Genome Res.* 2003;13: 103–107.
- 506 28. Kielbasa SM, Wan R, Sato K, Horton P, Frith MC. Adaptive seeds tame genomic sequence
507 comparison. *Genome Res.* 2011;21: 487–493.
- 508 29. Kent WJ, Baertsch R, Hinrichs A, Miller W, Haussler D. Evolution's cauldron: duplication,

- 509 deletion, and rearrangement in the mouse and human genomes. *Proc Natl Acad Sci United*
510 *States Am.* 2003;100: 11484–11489.
- 511 30. International Glossina Genome Initiative. Genome sequence of the tsetse fly (*Glossina*
512 *morsitans*): vector of African trypanosomiasis. *Sci.* 2014;344: 380–386.
- 513 31. Engström PG, Fredman D, Lenhard B. Ancora: a web resource for exploring highly
514 conserved noncoding elements and their association with developmental regulatory genes.
515 *Genome Biol.* 2008;9: R34.
- 516 32. Reim I, Mohler JP, Frasch M. Tbx20-related genes, mid and H15, are required for tinman
517 expression, proper patterning, and normal differentiation of cardioblasts in *Drosophila*.
518 *Mech Dev.* 2005;122: 1056–1069.
- 519 33. Yu G, Wang L-G, Han Y, He Q-Y. clusterProfiler: an R package for comparing biological
520 themes among gene clusters. *Omics: J Integr Biol.* 2012;16: 284–287.
- 521 34. Nepveu A. Role of the multifunctional CDP/Cut/Cux homeodomain transcription factor in
522 regulating differentiation, cell growth and development. *Gene.* 2001;270: 1–15.
- 523 35. Cameron RA, Samanta M, Yuan A, He D, Davidson E. SpBase: the sea urchin genome
524 database and web site. *Nucleic acids Res.* 2009;37: D750–D754.
- 525 36. Chiang CWK, Derti A, Schwartz D, Chou MF, Hirschhorn JN, Wu C-T. Ultraconserved
526 elements: analyses of dosage sensitivity, motifs and boundaries. *Genetics.* 2008;180:
527 2277–2293.
- 528 37. Walter K, Abnizova I, Elgar G, Gilks WR. Striking nucleotide frequency pattern at the
529 borders of highly conserved vertebrate non-coding sequences. *Trends Genet TIG.* 2005;21:
530 436–440.
- 531 38. Sheffield NC, Bock C. LOLA: enrichment analysis for genomic region sets and regulatory
532 elements in R and Bioconductor. *Bioinforma.* 2016;32: 587–589.
- 533 39. Gel B, Díez-Villanueva A, Serra E, Buschbeck M, Peinado MA, Malinverni R. regioneR: an
534 R/Bioconductor package for the association analysis of genomic regions based on
535 permutation tests. *Bioinforma.* 2016;32: 289–291.
- 536 40. Chiang CWK, Liu C-T, Lettre G, Lange LA, Jorgensen NW, Keating BJ, et al.
537 Ultraconserved elements in the human genome: association and transmission analyses of
538 highly constrained single-nucleotide polymorphisms. *Genetics.* 2012;192: 253–266.

Figure 1

bioRxiv preprint doi: <https://doi.org/10.1101/575704>; this version posted March 12, 2019. The copyright holder for this preprint (which was not certified by peer review) is the author/funder, who has granted bioRxiv a license to display the preprint in perpetuity. It is made available under aCC-BY 4.0 International license.



B Axt alignment



Figure 2

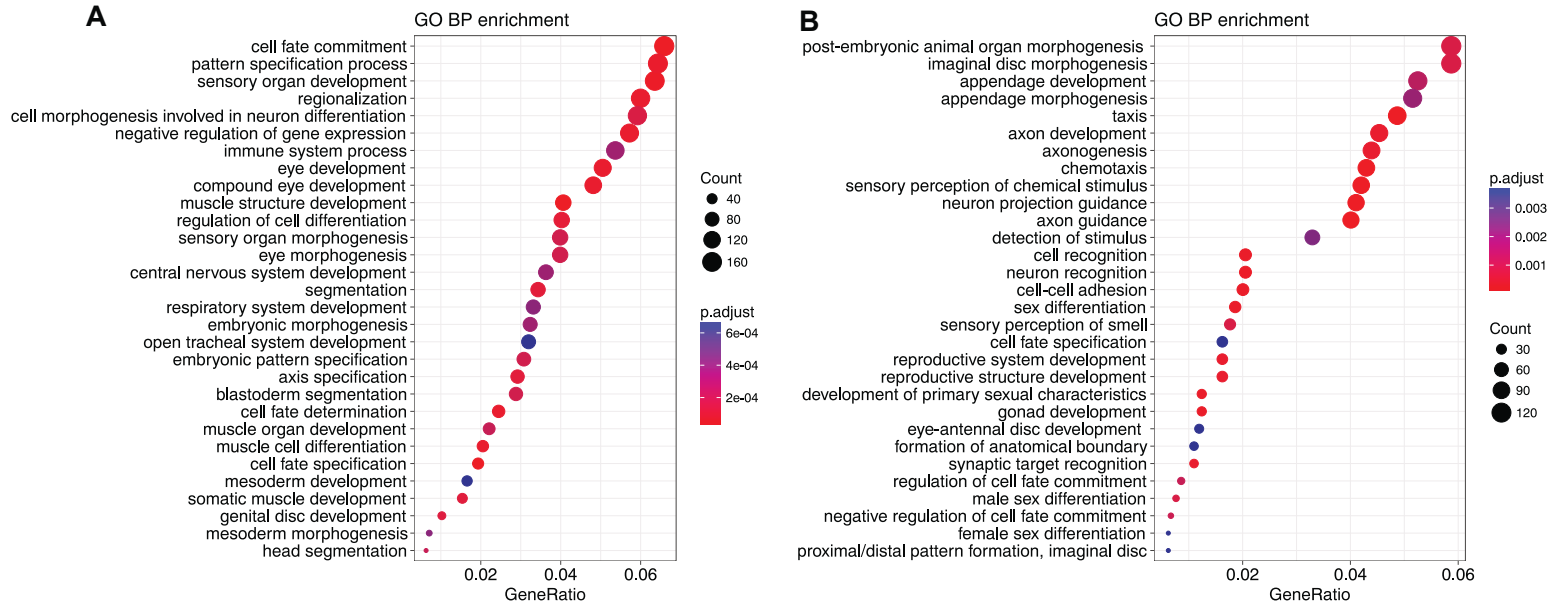


Figure 4

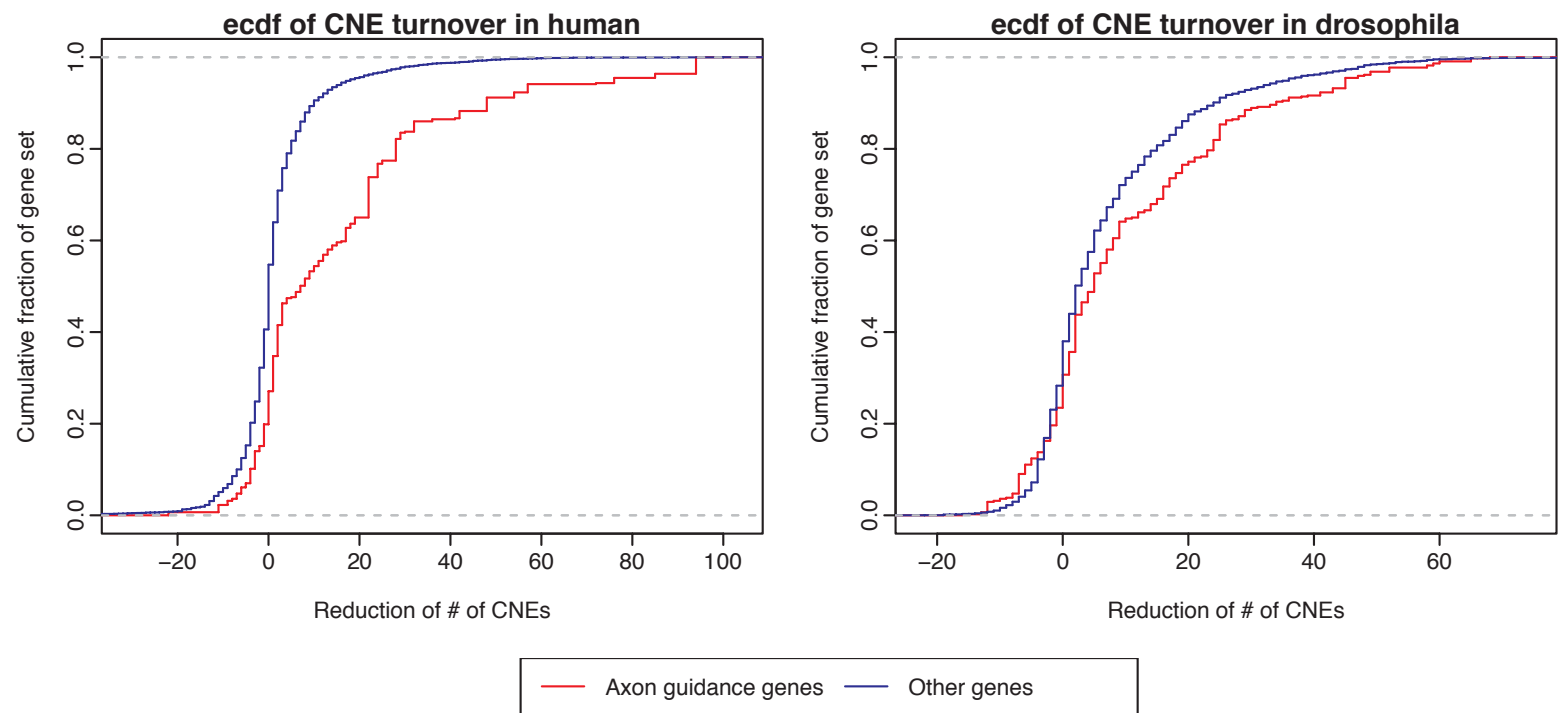


Figure 5

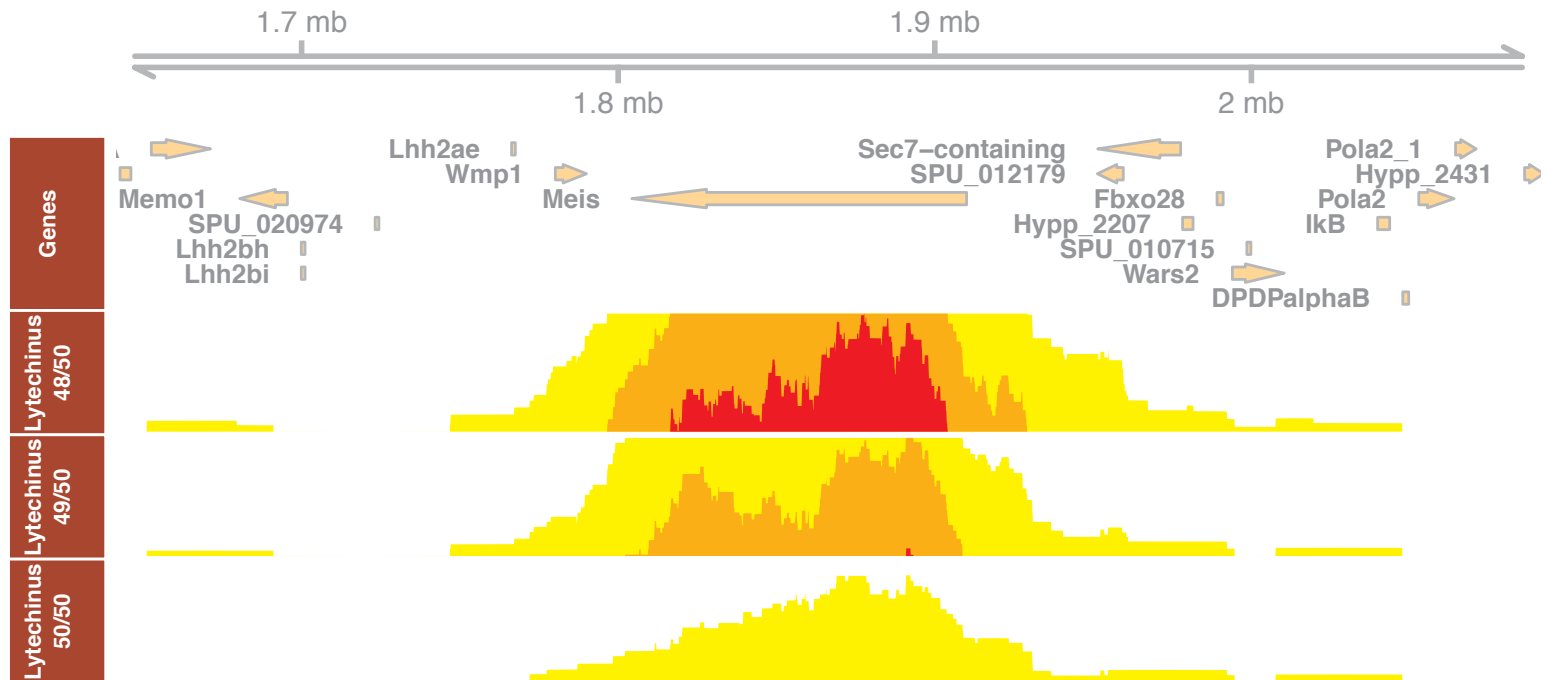


Figure 6

